

Removal of Bisphenol S from Aqueous Solution using Activated Carbon Derived from Rambutan Peel via Microwave Irradiation Technique

(Penyingkiran Bisfenol S daripada Larutan Akuas menggunakan Karbon Teraktif Terbitan daripada Kulit Rambutan melalui Teknik Penyinaran Gelombang Mikro)

AZRINA AZIZ, MOHAMAD FIRDAUS MOHAMAD YUSOP & MOHD AZMIER AHMAD*

School of Chemical Engineering, Engineering Campus, Universiti Sains Malaysia, 14300 Nibong Tebal, Penang, Malaysia

Received: 30 March 2022/Accepted: 19 August 2022

ABSTRACT

Bisphenol S (BPS) was introduced to replace Bisphenol A (BPA) in plastic production. Unfortunately, recent studies have shown that BPS is toxic. This study explores the conversion of rambutan peel into rambutan peel-based activated carbon (RPAC) via the economic route of single-stage microwave irradiation technique at radiation power and radiation time of 440 W and 6 min, respectively, under CO₂ gasification. The resulted RPAC posed BET surface area of 402.68 m²/g, mesopores surface area of 332.98 m²/g, total pore volume of 0.23 cm³/g, and average pore diameter of 2.26 nm, which lies in the mesopores region. The surface of RPAC was filled with various functional groups such as methylene, aliphatic fluoro, phenol, nitro, and alkyl compounds. Adsorption of BPS onto RPAC achieved equilibrium faster at lower BPS initial concentration as compared to the higher ones. Isotherm study found that the Langmuir model suits this adsorption process the best with a maximum monolayer adsorption capacity of 27.89 mg/g whereas the kinetic study showed that pseudo-second order (PSO) represented the kinetic data the best. Intraparticle diffusion plots suggested that the adsorption process consisted of three regions and each region was controlled by a different type of diffusion mechanism. Boyd plot confirmed that film diffusion was responsible for the slowest step in the adsorption process whilst thermodynamic parameters disclosed that adsorption of BPS onto RPAC was spontaneous, exothermic, governed by physisorption, and the randomness of the adsorption process was found to reduce at the solid-liquid interface.

Keywords: Activated carbon; adsorption process; bisphenol S; *Nephelium lappaceum* L.; microwave heating

ABSTRAK

Bisfenol S (BPS) telah diperkenalkan untuk menggantikan Bisfenol A (BPA) dalam penghasilan plastik. Namun, kajian terkini mendapati BPS juga bersifat toksik. Kajian ini menerokai penghasilan karbon teraktif berasaskan kulit rambutan (RPAC) daripada kulit rambutan melalui proses pemanasan sinaran gelombang mikro satu langkah yang menjimatkan pada kuasa dan masa pengaktifan masing-masing pada 440 W dan 6 minit di bawah aliran karbon dioksida, CO₂. RPAC yang terhasil memiliki luas permukaan BET 402.68 m²/g, luas permukaan liang meso 332.98 m²/g, jumlah isi padu liang 0.23 cm³/g dan purata diameter liang 2.26 nm, yang terletak di dalam julat liang meso. Permukaan RPAC terdapat pelbagai kumpulan berfungsi seperti metilena, fluoro alifatik, fenol, nitro dan sebatian alkil. Penjerapan BPS oleh RPAC mencapai keseimbangan lebih pantas pada kepekatan BPS yang lebih rendah berbanding yang lebih tinggi. Kajian isoterma mendapati proses penjerapan mengikuti model garis suhu Langmuir terbaik dengan kapasiti penjerapan 27.89 mg/g manakala kajian kinetik mendapati pseudo tertib kedua mengikuti data kinetik yang terbaik. Plot resapan intrazarah mencadangkan proses penjerapan terbina daripada tiga bahagian dan setiap bahagian dikawal oleh mekanisme resapan yang berbeza. Plot Boyd mengesahkan resapan filem bertanggungjawab sebagai langkah terlambat di dalam proses penjerapan manakala parameter termodinamik mengesahkan penjerapan BPS oleh RPAC berlaku secara spontan, eksotermik, dikawal oleh fisiserapan dan kerawakan proses penjerapan didapati berkurang antara muka pepejal-cecair.

Kata kunci: Bisfenol S; karbon teraktif; *Nephelium lappaceum* L., pemanasan gelombang mikro; proses penjerapan

INTRODUCTION

The existence of endocrine-disrupting chemicals (EDCs) in the environment has caused a great problem for the authorities to provide a good water quality supply to the citizens. In the beginning, the manufacturing industries of polycarbonate plastics and epoxy resins were dominated by Bisphenol A (BPA, 4,4'-dihydroxy-2,2-diphenylpropane) (Kim et al. 2022). But due to the harmful effects carried by BPA such as altering many metabolic reactions and causing reproductive impairment (Akash, Sabir & Rehman 2020), an alternative substance known as Bisphenol S (BPS, 4,4'-sulfonyldiphenol) was introduced to replace BPA. Unfortunately, data collected by scientists suggested that BPS is as toxic as BPA. According to An et al. (2021), BPS promotes a negative effect on steatosis and obesity processes, besides being responsible for disturbing the metabolism of mice, zebrafish, rats, and other species. Some studies also showed that BPS can cause a severe threat to the activities of anti-androgenic and estrogenic besides posing an adverse effect on the expression of the gene and carcinogenic towards organisms (Rezg et al. 2019; Song et al. 2019). Even worse, the existence of the sulfonyl group in BPS's structure causes its biodegradation and removal from the environment to be more challenging as compared to BPA (Frankowski et al. 2021).

Therefore, many methods of wastewater treatment are ventured out to provide safe clean drinking water to humans such as fluidized-bed bioreactor (Tabiś, Boroń & Bizon 2020), magnetotactic bacteria (Ali et al. 2018), membrane process (Yang et al. 2021), and bio-sorbents (Mohammed et al. 2020). Among these methods, the adsorption process using activated carbon (AC) can be regarded as one of the most effective techniques for water purification (Fahim Chyad et al. 2021). Nowadays, AC is widely used in a home-based water filtration unit to filter out contaminants and foreign objects from tap water thus enabling people to get safe water access and safe drinking water. AC is popular due to its many advantages such as (i) relatively low operational cost, (ii) simple in design without the need for special treatment units, (iii) effective to treat pollutants in a vast range of concentrations, and (iv) posing high surface area up to 2000 m²/g which is very beneficial in providing sites for adsorption process to take place. Another supremacy of AC is its versatility in treating a wide range of pollutants namely dyes (Ahmad et al. 2021c, 2017; Yusop et al. 2021), heavy metals (Yao et al. 2021), carbon dioxide, CO₂ gas (Othman, Yusof & Ismail 2020; Ramezanipour Penchah, Ghaemi & Jafari

2021; Soleimanpour et al. 2021; Zhang et al. 2018), phenol (Benmahdi et al. 2019), pharmaceutical products (El Maataoui et al. 2019; Moral-Rodríguez et al. 2019), pesticide (Aziz et al. 2021), and ammonia (Choi et al. 2020).

The worldwide demand for AC was found to be as minimum as 1,100,000 metric tons, and this value is predicted to rise 10% per year in the future (Fahim Chyad et al. 2021). Unfortunately, it is common for commercial AC to be produced from non-renewables and expensive raw materials such as lignite and bituminous coal. This is bad for the environment since the mining process to collect the coal itself is an extremely air, water, and land-polluted process. This is due to the emission of hydrogen sulfide, H₂S, carbon monoxide, CO, carbon dioxide, CO₂, methane, CH₄, nitrous oxide, NO_x, sulfur dioxide, SO₂, and the promotion of soil erosion and flooding during the coal mining process. To avoid these negative impacts, researchers are more interested to use agrowaste as AC's precursor such as *Gleditsia triacanthos* (Mathangi, Kalavathy & Miranda 2021), sunflower seed (Bahiraei & Behin 2021), potato peel (Osman et al. 2019), pomegranate peel (Ahmad et al. 2021a), coconut shell (Yusop, Jaya & Ahmad 2022b; Yusop et al. 2022c), and *Alpinia galanga* stem (Ahammad et al. 2021). Agrowastes are a good precursor for AC production because their surface is filled with different types of functional groups, thus improving their adsorption capability. By converting these agrowastes into AC, it can prevent farmers from burning them, a process that can cause air pollution and haze problems. Heat treatment onto precursor using conventional furnaces has been practiced for so long to produce AC. The conventional furnace transfers heat from the heating element to the sample via the conduction process, a process that consumes more energy and time. To combat this, the microwave irradiation technique has gained popularity among researchers due to its ability to provide a fast heating process without compromising the quality of the resulted AC (Yusop et al. 2022a). Agrowastes are known to be suitable to be activated via microwave heating due to their ability to absorb microwave energy, causing the electron in their structure to vibrate vigorously, thus dissipating heat that heated the sample from the inside to the outside. In this study, the peel from rambutan (*Nephelium lappaceum* L.) fruit was selected as the precursor to be converted into rambutan peel-based AC (RPAC) via microwave irradiation technique to scavenge the toxic BPS from an aqueous solution. This tropical fruit belongs to the family

of *Sapindaceae*, native to Southeast Asia and widely planted in tropical countries (Hernández-Hernández et al. 2019). Rambutan fruit can be consumed in its raw form or processed into becoming jam, pastry, and cake filling. According to Torgbo et al. (2022), rambutan peel is rich in the phenolic compound and for every 1 kg of rambutan fruit being processed, 459 to 647 grams of rambutan peel is discarded as waste (Rakariyatham et al. 2020).

MATERIALS AND METHODS

MATERIALS

BPS was purchased from Sigma Aldrich (M) Sdn. Bhd. whilst activation gas, CO₂ (99.90% purity) was supplied by MOX Gases Berhad, Malaysia. Rambutan peel was collected from a local market located in Nibong Tebal, Malaysia.

PREPARATION OF RPAC

The collected rambutan peel was washed thoroughly with tap water to remove dirt and impurities on them. Wet rambutan peel was kept inside an oven for 1 day at 110°C to allow them to dry. Once completely dried, the rambutan peel was ground into smaller pieces, and then, they were loaded inside the quartz test tube. The quartz test tube was placed inside an adjusted microwave oven (EMW2001W, Sweden). N₂ gas was allowed to flow inside the test tube for 2 min to remove the oxygen gas. Then, N₂ gas was switched to CO₂ gas at a flowrate of 150 cm³/min, and the sample was heated at a radiation power of 440 W and a radiation time of 6 min. The sample was allowed to cool down to room temperature under the flow of N₂ gas before they were taken out from the quartz test tube. The resulted sample of rambutan peel-based AC (RPAC) was kept inside an air-tight container to be used later in adsorption studies. The determination of RPAC's yield was conducted by applying the formula (1) given below:

$$Yield = \frac{W_f}{W_i} \times 100\% \quad (1)$$

where W_i is the dry weight of rambutan peel while W_f is the dry weight of RPAC.

CHARACTERIZATION SYSTEMS

In this study, several characterizations were done on the samples namely surface area, elemental analysis, surface morphology, and surface chemistry. Brunauer-

Emmet-Teller (BET) surface area, mesopores surface area, total pore volume together with average pore diameter were determined using a volumetric adsorption analyzer (Micromeritics ASAP 2020) which worked based on N₂ gas adsorption at a temperature of 77 K. Scanning electron microscopy (SEM) image of samples with 1000x magnification were taken using a scanning electron microscope (LEO SUPRA 55VP, Germany). The elemental composition of the samples was determined by using a simultaneous thermal analyzer (STA) (Model Perkin Elmer STA 6000, USA), and functional groups on the samples' surface were verified using Fourier transform infrared spectroscopy (FTIR) (IR Prestige 21 Shimadzu, Japan).

BATCH ADSORPTION STUDIES EQUILIBRIUM STUDY

To understand the effect of contact time, different initial concentrations, pH solution, and solution temperature on BPS removal, an equilibrium study was performed. BPS solution with 6 different concentrations of 5, 10, 15, 20, 25, and 30 mg/L was prepared and placed inside conical flasks. These conical flasks were assembled inside water bath shaker to give homogenous mixing to the solution. 0.2 g of RPAC was added inside each one of these flasks. Other conditions such as pH solution, solution temperature, and agitation speed were fixed at the original pH, 30 °C and 150 rpm, respectively. A small sample of BPS solution was withdrawn every hour until an equilibrium state was achieved, to check for its concentration using UV-Visible spectrophotometry (Model Shimadzu UV-1800, Japan) at a wavelength of 245 nm. The following equations were used to calculate BPS uptakes and BPS percentage removal, respectively:

$$q_e = \frac{(C_o - C_e)V}{M} \quad (2)$$

$$Removal (\%) = \frac{(C_o - C_e)}{C_o} \times 100\% \quad (3)$$

where q_e , C_o , C_e , V , and M denotes the amount of BPS adsorbed by RPAC at equilibrium (mg/g), initial concentration of BPS solution (mg/L), the equilibrium concentration of BPS solution (mg/L), the volume of BPS solution (mL) and weight of RPAC used (g), respectively. To study the effect of pH solution, 0.1 M NaOH and HCl were used to alter the pH of the BPS solution to be 2, 4, 6, 8, 10, and 12. Other conditions

such as BPS concentration, solution volume, solution temperature, and adsorbent dose were fixed at 100 mg/L, 200 mL, 30 °C, and 0.2 g, respectively. On the other hand, the effect of solution temperature was performed by changing the solution temperature to 30, 40, and 50°C, while the pH solution was fixed at the original value. Other conditions similar to the study of the pH effect were employed in the study of the temperature effect.

ISOTHERM STUDY

To recognize the relationship between the adsorbate in the bulk phase and the solid phase, an isotherm study was carried out. Similar to the equilibrium study, 6 BPS solutions between 2 and 12 mg/L were employed in the isotherm study. Other conditions such as RPAC weight, the volume of BPS solution, and pH solution were fixed to be 0.20 g, 200 mL, and original value, respectively. However, BPS concentration was only determined once, when the equilibrium point has been reached. In this study, the equilibrium phase of the BPS-RPAC adsorption system occurred at 8 h. Isotherm study was conducted at three different solution temperatures of 30, 40, and 50 °C. Four isotherm models (Langmuir, Freundlich, Temkin and Koble-Corrigan) were utilized. The non-linear equations for these isotherm models were solved using Microsoft Excel Solver 2016 and are given as follows:

Langmuir (Langmuir 1918):

$$q_e = \frac{Q_m K_L C_e}{1 + K_L C_e} \quad (4)$$

Freundlich (Freundlich 1906):

$$q_e = K_F C_e^{1/n_F} \quad (5)$$

Temkin (Temkin & Pyzhev 1940):

$$q_e = \frac{RT}{B} \ln(AC_e) \quad (6)$$

Koble-Corrigan (Koble & Corrigan 1952):

$$q_e = \frac{A_{KC} C_e^{n_{KC}}}{1 + B_{KC} C_e^{n_{KC}}} \quad (7)$$

where Q_m is maximum adsorption capacity; K_L is the constant of Langmuir; K_F and n_F are constants of Freundlich; B and A are constants of Temkin; A_{KC} , B_{KC} , and n_{KC} are constants for Koble Corrigan, R is

the universal gas constant and T is temperature. The correlation coefficient, R^2 , and root squared mean error (RSME) were judged to decide which model fitted the adsorption data the best. RSME was calculated using the following equation (Marrakchi et al. 2020):

$$RMSE = \sqrt{\frac{1}{n-1} \sum_{n=1}^n (q_{e,exp,n} - q_{e,cal,n})^2} \quad (8)$$

KINETIC STUDY

An almost identical procedure as in the equilibrium study was conducted to gather the kinetic information of the BPS-RPAC adsorption system. Unlike the equilibrium study, the sample was taken out to determine its concentration at a pre-determined time interval between 15 and 180 min. BPS solution with 6 different initial concentrations of 5, 10, 15, 20, 25, and 30 mg/L was used. Other conditions used in the kinetic study were as follows; an adsorbent dose of 0.2 g, solution volume of 200 mL, solution temperature of 30 °C, original pH solution with no alteration, and agitation speed of 150 rpm. The kinetic models utilized to test the kinetic data were pseudo-first order (PFO), pseudo-second order (PSO), intraparticle diffusion, and Boyd plot, and their equations are provided as follows:

PFO (Lagergren & Svenska 1898):

$$q_t = q_e [1 - \exp(-k_1 t)] \quad (9)$$

PSO (Ho & McKay 1999):

$$q_t = \frac{k_2 q_e^2 t}{1 + k_2 q_e t} \quad (10)$$

Intraparticle diffusion (Boopathy et al. 2013):

$$q_t = k_{t,i} t^{\frac{1}{2}} \quad (11)$$

Boyd plot (Islam et al. 2017):

$$B_t = -0.4977 - \ln \left(1 - \frac{q_t}{q_e} \right) \quad (12)$$

where k_1 is rate constant for PFO, k_2 is rate constant for PSO and $k_{t,i}$ is rate constant for intraparticle diffusion.

THERMODYNAMIC STUDY

The behaviour of the adsorption process under different

solution temperatures can be verified by understanding the thermodynamic parameters. Change of enthalpy, ΔH° , and change of entropy, ΔS° can be computed using the Van't Hoff equation as follows:

$$\ln K_c = \frac{\Delta S^\circ}{R} - \frac{\Delta H^\circ}{RT} \quad (13)$$

K_c is a dimensionless equilibrium constant that can be calculated using the following equation (Lima et al. 2019):

$$K_c = \frac{1000 \frac{mg}{g} \times K_L \times \text{molecular weight of adsorbate} \times [\text{adsorbate}]^\circ}{\gamma} \quad (14)$$

where $[\text{adsorbate}]^\circ$ and γ are the standard concentration of the adsorbate, which concentration by definition is 1 mol/L at standard conditions and coefficient of activity of the adsorbate (dimensionless), respectively. Other thermodynamic parameters such as Gibbs free energy, ΔG° , and activation energy, E_a can be computed using the following formulas, respectively:

$$\Delta G^\circ = -RT \ln K_c \quad (15)$$

$$\ln k_2 = \ln A - \frac{E_a}{RT} \quad (16)$$

where R is the universal gas constant ($8.314 \text{ J mol}^{-1} \text{ K}^{-1}$), T is absolute temperature, k_2 is the rate constant of PSO and A is the Arrhenius factor. In this study, all experimental were conducted three times and the average values were used.

RESULTS AND DISCUSSION

CHARACTERISTICS OF RPAC

The first characterization of samples was made in terms of surface area and pore characteristics. A significant increment from 0.78 to 402.68 m^2/g and from 0.01 to 332.98 m^2/g for BET surface area and mesopores surface area, respectively, were noticed after the rambutan peel was successfully converted into RPAC. Carbon-based materials like rambutan peel absorb microwave energy during the microwave irradiation step and generated a huge amount of energy that heated the sample. The heating process which is sourced from the vibration of an electron at an extremely high rate caused moisture, volatile matter (lignin, cellulose, and hemicellulose), and tar compounds to evaporate and

leaves the sample. The sample was left with many vacant sites or also known as pores, thus increasing the total pore volume from 0.0001 in a precursor to 0.23 cm^3/g in RPAC. The average pore in the precursor was 0.89 nm which reflected the domination of micropores type of pores in it. During the activation process, CO_2 molecules diffused deep into the carbon matrix and bombarded its surrounding, an action that creates more pores and increases the surface area to even higher. As the result, the pores in RPAC were shifted to the mesopores region (2.26 nm).

The next characterization was proximate analysis. The fixed carbon in rambutan peel was found to be 18.96% which can be considered relatively high for biomass. Therefore, the selection of rambutan peel as the precursor in this study was the right decision in the first place. The microwave irradiation technique was proven to be effective in removing moisture and volatile matter in the precursor. Therefore, moisture and volatile matter decreased sharply from 20.52 to 11.04% and from 45.85 to 26.21%, respectively, after the activation process took place. On contrary, fixed carbon increased significantly from 18.96 in the precursor to 55.02% in RPAC. A high percentage of fixed carbon is desired as they made up the matrix structure inside RPAC. Last but not least, the ash percentage of RPAC was found to be below 10% (7.73%) which is a good characteristic for AC since ash does not contain any pores, thus unable to promote the adsorption process at all.

Figures 1(a) and 1(b) provide the SEM image for rambutan peel and RPAC, respectively. Observation showed that no pores can be seen on the surface of the rambutan peel. This was predicted since the physical trait of rambutan peel is hard, an indication that it is not porous in its natural state. On the other hand, plenty of pores can be spotted on RPAC's SEM image and these pores were found to be dispersed everywhere randomly. Before the activation process via microwave heating, these pores were occupied by tar and volatile matter that comprised lignin, cellulose, and hemicellulose components. Due to their inability to withstand high temperatures, they condensed and leave empty spaces behind which later, evolved into pores (Yusop et al. 2021). Gasification of CO_2 on these pores caused their size to increase and change the type of pores from micropores to mesopores.

FTIR spectrums for rambutan peel and RPAC are given in Figure 2 whilst Table 1 shows the summary of bandwidth with their respective functional groups.

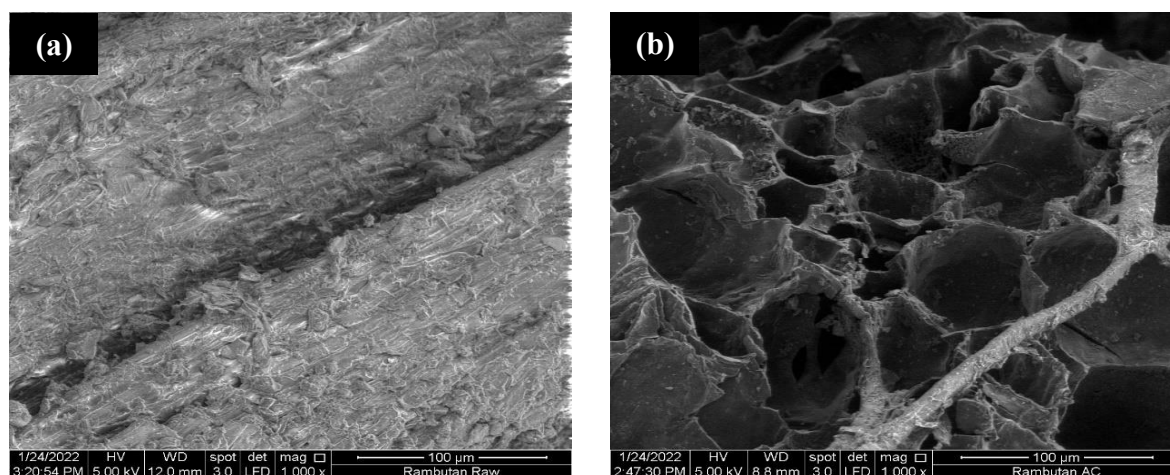


FIGURE 1. SEM image for (a) rambutan peel and (b) RPAC at magnification level of 1000×

As expected, the rambutan peel contains more peaks as compared to the RPAC. Several peaks were noticed to exist on both rambutan peel and RPAC such as aliphatic fluoro compound (C-F stretch), phenol (C-O stretch), aromatic nitro compound, C≡C terminal alkyl, and methylene (C-H asymmetric stretch). The molecular alteration effect by microwave irradiation technique can be observed when an aromatic nitro compound in rambutan peel was reduced to an aliphatic nitro compound

in RPAC and methylene C-H asymmetric stretch in rambutan peel was converted to methylene $-(CH_2)_n-$ rocking ($n \geq 3$) in RPAC. Some functional groups were unable to survive microwave heating, thus their peaks are only visible in rambutan peel. These functional groups are aromatic primary amine (CN stretch), carbonate ions, alkenyl C=C stretch, and hydroxy group, H-bonded OH stretch.

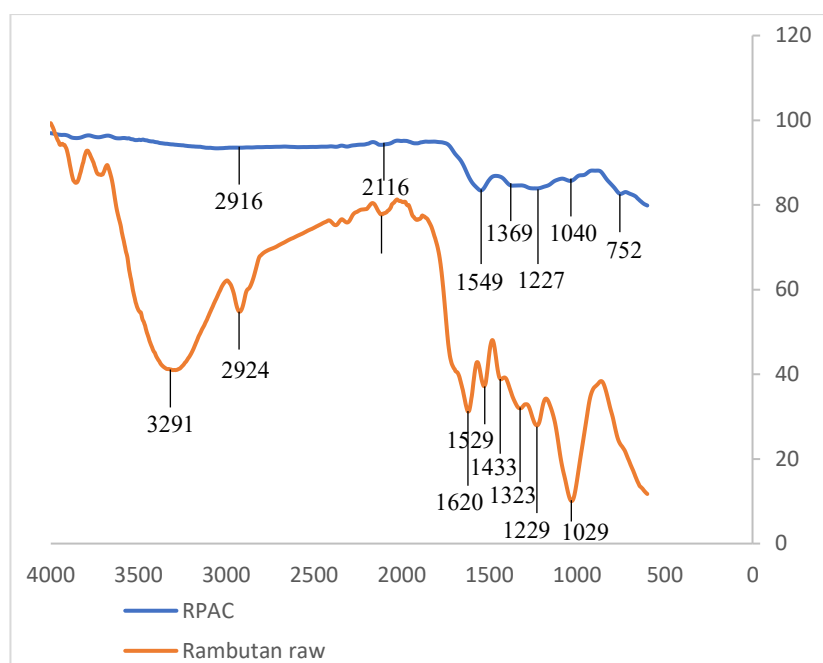


FIGURE 2. FTIR spectrums for rambutan peel and RPAC

TABLE 1. Summary of FTIR peaks for rambutan peel and RPAC

| Rambutan peel | | RPAC | |
|--------------------------|--|--------------------------|--|
| Peak (cm ⁻¹) | Functional groups | Peak (cm ⁻¹) | Functional groups |
| 1029 | Aliphatic fluoro compound, C-F stretch | 752 | Methylene —(CH ₂) _n — rocking (n ≥ 3) |
| 1229 | Phenol, C-O stretch | 1040 | Aliphatic fluoro compound, C-F stretch |
| 1323 | Aromatic primary amine, CN stretch | 1227 | Phenol, C-O stretch |
| 1433 | Carbonate ions | 1369 | Aliphatic nitro compound |
| 1529 | Aromatic nitro compound | 1549 | Aromatic nitro compound |
| 1620 | Alkenyl C=C stretch | 2116 | C≡C terminal alkyl (monosubstituted) |
| 2117 | C≡C terminal alkyl (monosubstituted) | 2916 | Methylene C-H asymmetric stretch |
| 2924 | Methylene C-H asymmetric stretch | | |
| 3291 | Hydroxy group, H-bonded OH stretch | | |

ADSORPTION EQUILIBRIUM

Figure 3(a) provides the plots of BPS adsorption capacity against time whereas Figure 3(b) shows the plots of BPS removal percentage against time, for different initial solution concentrations. Both plots were observed to increase with time at the beginning of the adsorption process. Initially, RPAC was filled with many active sites which ready to be occupied by BPS molecules for the adsorption process to occur. After sometimes, they reached a static state or better known as the equilibrium state, which indicates that: (i) RSAC had reached its saturated level where no more BPS can be adsorbed, (ii) repulsion between BPS in the bulk phase and solid phase occurred strongly and (iii) the net rate of the adsorption-desorption process was equal to zero.

From Figure 3(a), it was noticed that it took a longer contact time for higher initial solution concentration to reach an equilibrium state as compared to lower initial solution concentration. To be precise, a lower initial concentration of 5, 10, and 15 mg/L required 3 h to attain equilibrium whereas a higher initial concentration

of 20, 25, and 30 mg/L needed 6 to 7 h to achieve theirs. This phenomenon can be explained by the fact that at a lower initial concentration, the number of BPS was small compared to the number of active sites available on the RSAC's surface. Therefore, the competition among BPS to be adsorbed was less intense. On contrary, the exact opposite was happening at higher initial concentration. As the initial solution concentration increased from 5 to 30 mg/L, the adsorption capacity of BPS was increased as well from 4.67 to 22.00 mg/g. This can be explained by the existence of a higher mass transfer driving force at a higher initial concentration that can overcome the mass transfer resistance that existed between BPS in the bulk phase and in solid phase, thus producing higher BPS adsorption capacity (Tharaneedhar et al. 2017).

From Figure 3(b), when the initial solution concentration increased from 5 to 30 mg/L, the BPS removal percentage dropped from 93.40 to 73.33%. At a lower initial concentration, the ratio of available surface area to the number of BPS molecules was high, therefore higher percentage of BPS can be removed.

However, at higher initial concentrations, the number of BPS molecules increased significantly but the number of active sites remained the same, thus resulting in lower percentage removal of BPS molecules. A similar trend

where the higher initial concentration of adsorbate had a positive effect on adsorption capacity and a negative effect on adsorbate percentage removal was observed in the study conducted by Ahmad et al. (2021b).

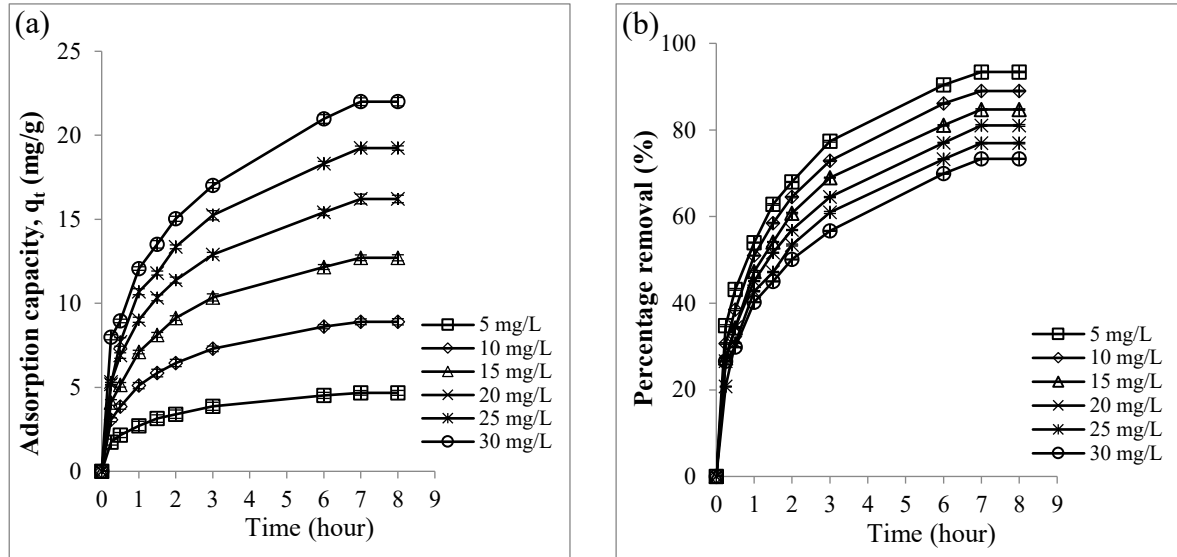


FIGURE 3. Plots of (a) BPS adsorption capacity and (b) BPS percentage removal versus adsorption time for different initial concentration at solution temperature of 30 °C

ADSORPTION ISOTHERM

The adsorption data was verified using four isotherm models (Langmuir, Freundlich, Temkin, and Koble-Corrigan) and the plots of these non-linear equations are given in Figure 4. In terms of RSME, Koble-Corrigan produced the lowest average value of 0.05. The low RSME value indicated that the isotherm model can predict the experimental equilibrium adsorption capacity with excellent accuracy. However, the n_{KC} value was found to be below 1 (0.60 - 0.91) for all three-solution temperatures, signifying that the Koble-Corrigan isotherm is not reliable to represent the BPS-RPAC adsorption system, despite the high R^2 and low RSME values (Koble & Corrigan 1952; Mozaffari Majd et al. 2022). Due to this, the Langmuir isotherm is the best model that fitted this adsorption process due to high R^2 and low RSME with an average value of 0.9995 and 0.37, respectively. Langmuir model indicated that adsorption of BPS onto RPAC formed a monolayer coverage and the active sites available on RPAC's surface were homogenous in nature. At a solution temperature of 30 °C, Langmuir monolayer adsorption capacity, Q_m was found to be 27.89

mg/g. This value was considered relatively moderate when compared to BPS removal by corn straw biochar (20.14 mg/g) (Yang et al. 2020) and porous β -cyclodextrin modified cellulose nano-fiber membrane (46.89 mg/g) (Lv et al. 2021).

ADSORPTION KINETIC

Kinetic models of pseudo-first order (PFO) and pseudo-second order (PSO) were utilized to understand the kinetic behavior of the BPS-RPAC adsorption system. Linearized plots of these models are given in Figures 5(a) and 5(b), respectively. At all three adsorption temperature systems studied (30, 40, and 50 °C), both kinetic models were found to produce good R^2 values (>0.98). Despite this, PSO was shown to describe the BPS-RPAC adsorption system much better than PFO since PSO produced significantly low RSME values between 0.46 to 1.30. PSO signified that chemisorption might be the rate-limiting step in the adsorption of BPS onto RPAC. To further confirm this assumption, intraparticle diffusion and Boyd plot were also studied in the next section.

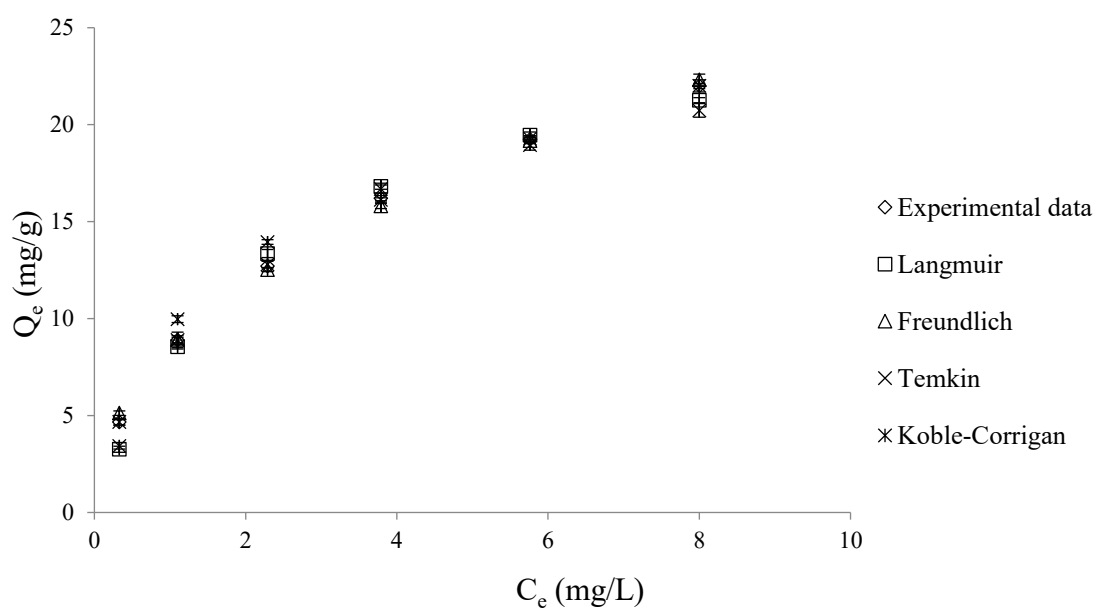


FIGURE 4. Non-linearized isotherm plots for BPS-RPAC adsorption system at 30 °C

Generally, a lower value of k_2 was obtained at the highest BPS concentration studied (30 mg/L) as compared to the lowest BPS concentration studied (5 mg/L). This trend

occurred because, at low BPS concentration, the ratio of adsorbate molecules: active sites was low, resulting in a faster adsorption process and higher rate constant, k_2 .

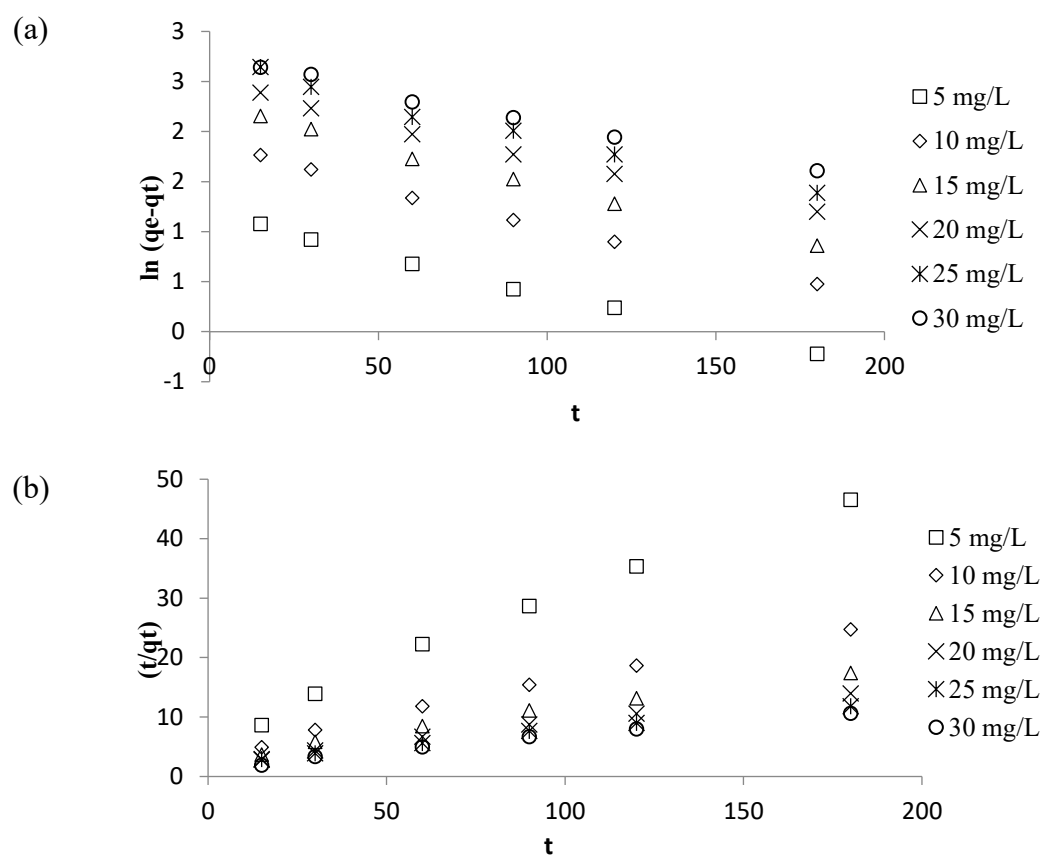


FIGURE 5. Plots of (a) PFO and (b) PSO for BPS-RPAC adsorption system at solution temperature of 30 °C

Intraparticle diffusion plots are provided in Figure 6 whereas all the parameters were summarized and tabulated in Table 2. Based on Figure 6, three distinct sections can be seen which implied that more than one mechanism was involved in the BPS-RPAC adsorption system. The first section ($t=0$ until $t=1.5$ h) represented the film layer diffusion where the adsorption of BPS onto RPAC's external surface involved strong electrostatic attraction. The second section ($t=1.5$ until $t=3$ h) was associated with a gradual adsorption process where its mechanism was controlled by intraparticle diffusion. In this section, BPS molecules diffused from the external layer of RPAC into the RPAC's internal pores. Boundary layer diffusion in the first section was the dominant mechanism as compared to the pores diffusion in the second section since at all BPS concentrations studied, k_{d1} values were higher than k_{d2} values. The third section

($t=3$ until $t=7$ h) corresponded to a stage where an equilibrium state was about to be achieved. At this point, available active sites were exceptionally low and the repulsion force between BPS molecules in the bulk phase and solid phase were at the maximum value, thus lower k_{d3} values were obtained as compared to k_{d1} and k_{d2} , at all BPS concentrations studied. For all three sections, C_i values were observed to be higher at the highest BPS concentration studied (30 mg/L) than the C_i values in the lowest BPS concentration studied (5 mg/L), which signaled a higher boundary layer thickness at higher BPS concentration. Further determination on the slowest step in BPS adsorption onto RPAC was done by utilizing Boyd plots as shown in Figure 7. Based on the plots, all lines did not pass through the origin, which concluded that the film diffusion mechanism was the slowest step and governed the adsorption of BPS onto RPAC.

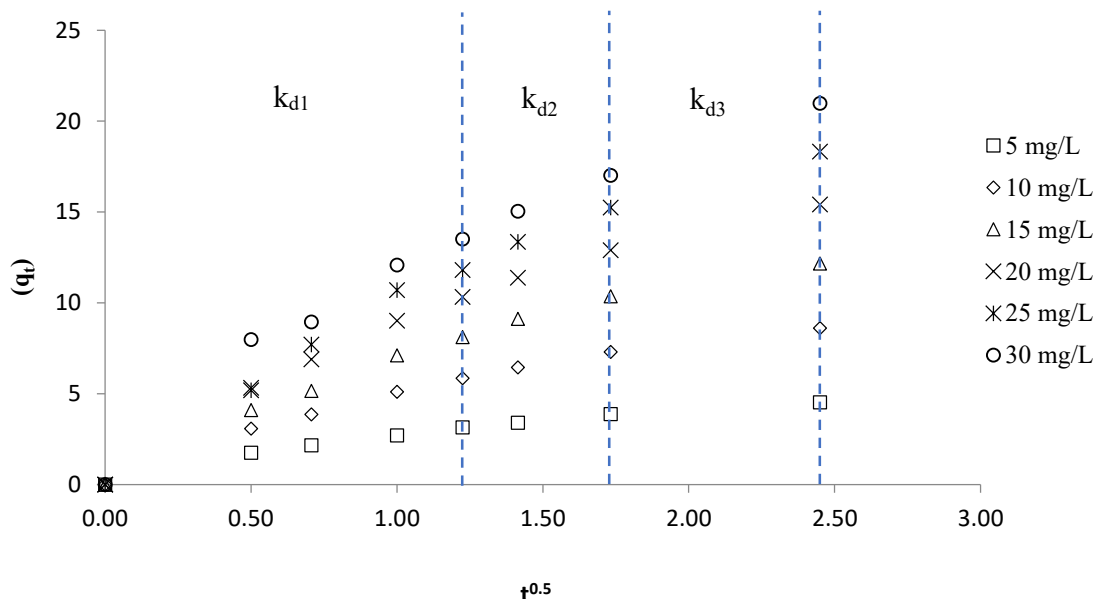


FIGURE 6. Plots of intraparticle diffusion for BPS-RPAC adsorption system at solution temperature of 30 °C

ADSORPTION THERMODYNAMIC

The adsorption capacity of BPS adsorbed by RPAC at different solution temperatures together with thermodynamic parameters was tabulated in Table 3. When the solution temperature increased from 30 to 50°C, the adsorption capacity of BPS was noticed to reduce from 22.00 to 19.01 mg/g, thus signaling an exothermic behavior. This result was consistent with the negative value of change of enthalpy, ΔH° (-42.59 kJ/mol), hence confirming the exothermic nature of the adsorption process. Gibbs free energy, ΔG° values were found to be -29.55, -29.12, and -28.69 kJ/mol for solution

temperatures of 30, 40, and 50°C, respectively. Negative values of ΔG° signified spontaneous adsorption process whereas the higher value of this parameter at higher solution temperature proved that adsorption of BPS onto RPAC was favored at lower solution temperature. The value of entropy change, ΔS° was disclosed to be -0.04 kJ/mol K) and the negative sign indicated the decreased adsorption randomness at the solid-liquid interface. Finally, Arrhenius activation energy, E_a was computed to be 17.80 kJ/mol, therefore verifying that the physisorption type of sorption contributed the most during the rate-limiting step in the adsorption process.

TABLE 2. Intraparticle diffusion parameters for BPS-RPAC adsorption system at 30 °C

| Parameters | BPS initial concentration (mg/L) | | | | | |
|------------|----------------------------------|--------|--------|--------|--------|--------|
| | 5 | 10 | 15 | 20 | 25 | 30 |
| k_{d1} | 2.5242 | 4.7588 | 6.6419 | 8.4314 | 9.9476 | 10.908 |
| C_1 | 0.2155 | 0.3077 | 0.3352 | 0.5249 | 0.2483 | 1.0148 |
| R^2_1 | 0.971 | 0.9827 | 0.9885 | 0.9838 | 0.9902 | 0.9626 |
| k_{d2} | 1.4431 | 2.8183 | 4.3414 | 5.0366 | 6.8299 | 6.6913 |
| C_2 | 1.3674 | 2.4238 | 2.8713 | 4.1983 | 5.2321 | 3.7174 |
| R^2_2 | 0.9996 | 0.9976 | 0.9927 | 0.9984 | 0.9952 | 0.9917 |
| k_{d3} | 0.8838 | 1.783 | 2.5667 | 3.5892 | 4.355 | 5.477 |
| C_3 | 2.3421 | 4.2089 | 5.8987 | 6.6718 | 7.6891 | 7.5289 |
| R^2_3 | 0.9992 | 0.9987 | 0.9996 | 0.9992 | 0.9997 | 0.9999 |

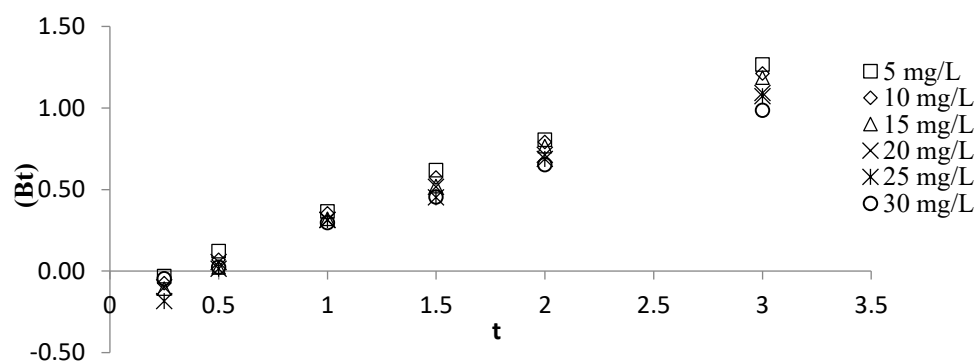


FIGURE 7. Boyd plots for BPS-RPAC adsorption system at solution temperature of 30 °C

TABLE 3. Adsorption capacity under different solution temperature and thermodynamic parameters for BPS-RPAC adsorption system

| | Adsorption capacity (mg/g) | ΔH° (kJ/mol) | ΔS° (kJ/mol K) | E_a (kJ/mol) | $^\circ G$ (kJ/mol) |
|----------|----------------------------|---------------------------|-----------------------------|----------------|---------------------|
| 303.15 K | 22.00 | | | | -29.55 |
| 313.15 K | 20.22 | -42.59 | -0.04 | 17.80 | -29.12 |
| 323.15 K | 19.01 | | | | -28.69 |

CONCLUSIONS

Rambutan peel was the right choice to be converted into AC to adsorb BPS due to its relatively high fixed carbon content of 18.96%. Single-step microwave irradiation technique at radiation power of 440 W and radiation time of 6 min succeeded in creating RPAC with relatively moderate BET surface area, mesopores surface area, and total pore volume of 402.68 m²/g, 332.98 m²/g, and 0.23 cm³/g, respectively. RPAC was dominated by mesopores type of pores since the average pore diameter was disclosed to be 2.26 nm. FTIR spectrum showed that many functional groups existed on the surface of RPAC which included methylene, aliphatic fluoro, phenol, nitro, and alkyl compounds. Adsorption equilibrium showed that lower BPS concentration (5 to 15 mg/L) took approximately 3 h to achieve an equilibrium state whereas the same state was attained by higher BPS concentration (20 to 30 mg/L) within 6 to 7 h. As the initial concentration increased from 5 to 30 mg/L, adsorption capacity and percentage removal of RBS were found to increase (4.67 to 22.00 mg/g) and decreased (93.40 to 73.33%), respectively. Isotherm and kinetic studies showed that the adsorption of BPS onto RPAC was best represented by Langmuir and PSO models, respectively, with maximum monolayer adsorption capacity, Q_m of 27.89 mg/g. Intraparticle diffusion plots suggested that the diffusion mechanisms involved more than one type of reaction whilst the Boyd plot confirmed that the rate-limiting step in the adsorption process was contributed by the film diffusion. Thermodynamic parameters of ΔH° , ΔS° , and E_a were found to be -42.59 kJ/mol, -0.04 kJ/mol.K, and 17.80 kJ/mol, respectively, therefore implying that the BPS-RPAC adsorption system was exothermic in nature, decreased randomness at the solid-liquid interface and controlled by physisorption type of adsorption, respectively. Negative values obtained for ΔG° (-29.55 to -28.69 kJ/mol) proved that the adsorption process was spontaneous in nature. All in all, the produced RPAC via the economic route of single-stage microwave irradiation technique was competitive in removing BPS from aqueous solution.

ACKNOWLEDGEMENTS

This research is supported by the Ministry of Higher Education Malaysia under the Fundamental Research Grant Scheme (project code: FRGS/1/2021/TK0/USM/01/3).

REFERENCES

- Ahammad, N.A., Yusop, M.F.M., Mohd Din, A.T. & Ahmad, M.A. 2021. Preparation of *Alpinia galanga* stem based activated carbon via single-step microwave irradiation for cationic dye removal. *Sains Malaysiana* 50(8): 2251-2269.
- Ahmad, M.A., Aswareusoff, M., Oladoye, P.O., Adegok, K.A. & Bell, O.S. 2021a. Optimization and batch studies on adsorption of Methylene blue dye using pomegranate fruit peel based adsorbent. *Chemical Data Collections* 32: 100676.
- Ahmad, M.A., Hamid, S.R.A., Yusop, M.F.M. & Aziz, H.A. 2017. Optimization of microwave-assisted durian seed based activated carbon preparation conditions for methylene blue dye removal. *AIP Conference Proceedings* 1892: 040019.
- Ahmad, M.A., Yusop, M.F.M., Zakaria, R., Karim, J., Yahaya, N.K.E.M., Mohamed Yusoff, M.A., Hashim, N.H.F. & Abdullah, N.S. 2021b. Adsorption of methylene blue from aqueous solution by peanut shell based activated carbon. *Materials Today: Proceedings* 47(6): 1246-1251.
- Ahmad, M.A., Yusop, M.F.M., Awang, S., Yahaya, N.K.E.M., Rasyid, M.A. & Hassan, H. 2021c. Carbonization of sludge biomass of water treatment plant using continuous screw type conveyer pyrolyzer for methylene blue removal. *IOP Conference Series: Earth and Environmental Science* 765: 012112.
- Akash, M.S.H., Sabir, S. & Rehman, K. 2020. Bisphenol A-induced metabolic disorders: From exposure to mechanism of action. *Environmental Toxicology and Pharmacology* 77: 103373.
- Ali, I., Peng, C., Khan, Z.M., Naz, I. & Sultan, M. 2018. An overview of heavy metal removal from wastewater using magnetotactic bacteria. *Chemical Engineering & Technology* 93: 2817-2832.
- An, H., Yu, H., Wei, Y., Liu, F. & Ye, J. 2021. Disrupted metabolic pathways and potential human diseases induced by bisphenol S. *Environmental Toxicology and Pharmacology* 88: 103751.
- Aziz, A., Khan, M.N.N., Yusop, M.F.M., Jaya, M.J.J., Jaya, M.A.T. & Ahmad, M.A. 2021. Single-stage microwave-assisted coconut-shell-based activated carbon for removal of dichlorodiphenyltrichloroethane (DDT) from aqueous solution: Optimization and batch studies. *International Journal of Chemical Engineering (Special Issue - Advances in Coagulation-Adsorption Processes)* 2021: 9331386.
- Bahiraei, A. & Behin, J. 2021. Effect of citric acid and sodium chloride on characteristics of sunflower seed shell-derived activated carbon. *Chemical Engineering & Technology* 44: 1604-1617.
- Benmahdi, F., Semra, S., Haddad, D., Mandin, P., Kolli, M. & Bouhelassa, M. 2019. Breakthrough curves analysis and statistical design of phenol adsorption on activated carbon. *Chemical Engineering & Technology* 42: 355-369.

- Boopathy, R., Karthikeyan, S., Mandal, A.B. & Sekaran, G. 2013. Adsorption of ammonium ion by coconut shell-activated carbon from aqueous solution: Kinetic, isotherm, and thermodynamic studies. *Environ. Sci. Pollut. Res. Int.* 20: 533-542.
- Choi, J.H., Jang, J.T., Yun, S.H., Jo, W.H., Lim, S.S., Park, J.H., Chun, I.S., Lee, J.-H. & Yoon, Y.I. 2020. Efficient removal of ammonia by hierarchically porous carbons from a CO₂ capture process. *Chemical Engineering & Technology* 43: 2031-2040.
- El Maataoui, Y., El M'rabet, M., Maaroufi, A. & Dahchour, A. 2019. Spiramycin adsorption behavior on activated bentonite, activated carbon and natural phosphate in aqueous solution. *Environmental Science and Pollution Research* 26: 15953-15972.
- Fahim Chyad, T., Fahim Chyad Al-Hamadani, R., Ageel Hammood, Z. & Abd Ali, G. 2021. Removal of zinc (II) ions from industrial wastewater by adsorption on to activated carbon produced from pine cone. *Materials Today: Proceedings* <https://doi.org/10.1016/j.matpr.2021.07.016>.
- Frankowski, R., Płatkiewicz, J., Stanisiz, E., Grześkowiak, T. & Zgoła-Grześkowiak, A. 2021. Biodegradation and photo-fenton degradation of bisphenol A, bisphenol S and fluconazole in water. *Environmental Pollution* 289: 117947.
- Freundlich, H.M.F. 1906. Over the adsorption in solution. *The Journal of Physical Chemistry* 57: 385-471.
- Hernández-Hernández, C., Aguilar, C.N., Rodríguez-Herrera, R., Flores-Gallegos, A.C., Morlett-Chávez, J., Govea-Salas, M. & Ascacio-Valdés, J.A. 2019. Rambutan (*Nephelium lappaceum* L.): Nutritional and functional properties. *Trends in Food Science & Technology* 85: 201-210.
- Ho, Y.S. & McKay, G. 1999. Pseudo-second order model for sorption processes. *Process Biochemistry* 34: 451-465.
- Islam, M.A., Sabar, S., Benhouria, A., Khanday, W.A., Asif, M. & Hameed, B.H. 2017. Nanoporous activated carbon prepared from karanj (*Pongamia pinnata*) fruit hulls for methylene blue adsorption. *Journal of the Taiwan Institute of Chemical Engineers* 74: 96-104.
- Kim, J.I., Lee, Y.A., Shin, C.H., Hong, Y.-C., Kim, B.-N. & Lim, Y.-H. 2022. Association of bisphenol A, bisphenol F, and bisphenol S with ADHD symptoms in children. *Environment International* 161: 107093.
- Koble, R.A. & Corrigan, T.E. 1952. Adsorption isotherms for pure hydrocarbons. *Industrial & Engineering Chemistry* 44: 383-387.
- Lagergren, S. & Svenska, K. 1898. About the theory of so-called adsorption of soluble substances. *Kungliga Svenska Vetenskapsakademiens Handlingar* 24: 1-39.
- Langmuir, I. 1918. The adsorption of gases on plane surfaces of glass, mica and platinum. *Journal of the American Chemical Society* 40: 1361-1403.
- Lima, E.C., Hosseini-Bandegharaci, A., Moreno-Piraján, J.C. & Anastopoulos, I. 2019. A critical review of the estimation of the thermodynamic parameters on adsorption equilibria. Wrong use of equilibrium constant in the Van't Hoof equation for calculation of thermodynamic parameters of adsorption. *Journal of Molecular Liquids* 273: 425-434.
- Lv, Y., Ma, J., Liu, K., Jiang, Y., Yang, G., Liu, Y., Lin, C., Ye, X., Shi, Y., Liu, M. & Chen, L. 2021. Rapid elimination of trace bisphenol pollutants with porous β -cyclodextrin modified cellulose nanofibrous membrane in water: Adsorption behavior and mechanism. *Journal of Hazardous Materials* 403: 123666.
- Marrakchi, F., Hameed, B.H. & Bouaziz, M. 2020. Mesoporous and high-surface-area activated carbon from defatted olive cake by-products of olive mills for the adsorption kinetics and isotherm of methylene blue and acid blue 29. *Journal of Environmental Chemical Engineering* 8: 104199.
- Mathangi, J.B., Kalavathy, M.H. & Miranda, L.R. 2021. Pore formation mechanism and sorption studies using activated carbon from *Gleditsia triacanthos*. *Chemical Engineering & Technology* 44: 892-900.
- Mohammed, E., Kamel, M., El Iraqi, K., Tawfik, A.M., Khattab, M.S. & Elsabagh, M. 2020. *Zingiber officinale* and *Glycyrrhiza glabra*, individually or in combination, reduce heavy metal accumulation and improve growth performance and immune status in *Nile tilapia*, *Oreochromis niloticus*. *Chemical Engineering & Technology* 51: 1933-1941.
- Moral-Rodríguez, A.I., Leyva-Ramos, R., Ania, C.O., Ocampo-Pérez, R., Isaacs-Páez, E.D., Carrales-Alvarado, D.H. & Parra, J.B. 2019. Tailoring the textural properties of an activated carbon for enhancing its adsorption capacity towards diclofenac from aqueous solution. *Environmental Science and Pollution Research* 26: 6141-6152.
- Mozaffari Majd, M., Kordzadeh-Kermani, V., Ghalandari, V., Askari, A. & Sillanpää, M. 2022. Adsorption isotherm models: A comprehensive and systematic review (2010-2020). *Science of The Total Environment* 812: 151334.
- Osman, A.I., Blewitt, J., Abu-Dahrieh, J.K., Farrell, C., Al-Muhtaseb, A.A.H., Harrison, J. & Rooney, D.W. 2019. Production and characterisation of activated carbon and carbon nanotubes from potato peel waste and their application in heavy metal removal. *Environmental Science and Pollution Research* 26: 37228-37241.
- Othman, F.E.C., Yusof, N. & Ismail, A.F. 2020. Activated-carbon nanofibers/graphene nanocomposites and their adsorption performance towards carbon dioxide. *Chemical Engineering & Technology* 43: 2023-2030.
- Rakariyatham, K., Zhou, D., Rakariyatham, N. & Shahidi, F. 2020. Sapindaceae (*Dimocarpus longan* and *Nephelium lappaceum*) seed and peel by-products: Potential sources for phenolic compounds and use as functional ingredients in food and health applications. *Journal of Functional Foods* 67: 103846.

- Ramezanipour Penchah, H., Ghaemi, A. & Jafari, F. 2022. Piperazine-modified activated carbon as a novel adsorbent for CO₂ capture: Modeling and characterization. *Environmental Science and Pollution Research* 29: 5134-5143.
- Rezg, R., Abot, A., Mornagui, B. & Knauf, C. 2019. Bisphenol S exposure affects gene expression related to intestinal glucose absorption and glucose metabolism in mice. *Environmental Science and Pollution Research* 26: 3636-3642.
- Soleimanpour, A., Farsi, M., Keshavarz, P. & Zeinali, S. 2021. Modification of activated carbon by MIL-53(Al) MOF to develop a composite framework adsorbent for CO₂ capturing. *Environmental Science and Pollution Research* 28: 37929-37939.
- Song, P., Fan, K., Tian, X. & Wen, J. 2019. Bisphenol S (BPS) triggers the migration of human non-small cell lung cancer cells via upregulation of TGF- β . *Toxicology in Vitro* 54: 224-231.
- Tabiś, B., Boroń, D. & Bizon, K. 2020. Biological water treatment by a hybrid fluidized-bed bioreactor: Theoretical study. *Chemical Engineering & Technology* 43: 983-994.
- Temkin, M.I. & Pyzhev, V. 1940. Kinetics and ammonia synthesis on promoted iron catalyst *Acta Physicochimica USSR* 12: 327-356.
- Tharaneedhar, V., Senthil Kumar, P., Saravanan, A., Ravikumar, C. & Jaikumar, V. 2017. Prediction and interpretation of adsorption parameters for the sequestration of methylene blue dye from aqueous solution using microwave assisted corncob activated carbon. *Sustainable Materials and Technologies* 11: 1-11.
- Torgbo, S., Sukatta, U., Kamonpatana, P. & Sukyai, P. 2022. Ohmic heating extraction and characterization of rambutan (*Nephelium lappaceum* L.) peel extract with enhanced antioxidant and antifungal activity as a bioactive and functional ingredient in white bread preparation. *Food Chemistry* 382: 132332.
- Yang, X., Liu, Y., Hu, S., Yu, F., He, Z., Zeng, G., Feng, Z. & Sengupta, A. 2021. Construction of Fe₃O₄@MXene composite nanofiltration membrane for heavy metal ions removal from wastewater. *Chemical Engineering & Technology* 32: 1000-1010.
- Yang, X., Zhang, S., Liu, L. & Ju, M. 2020. Study on the long-term effects of DOM on the adsorption of BPS by biochar. *Chemosphere* 242: 125165.
- Yao, L., Esmacili, H., Haghani, M. & Roco-Videla, A. 2021. Activated carbon/bentonite/Fe₃O₄ as a novel nanobiocomposite for high removal of Cr (VI) ions. *Chemical Engineering & Technology* 44: 1908-1918.
- Yusop, M.F.M., Ahmad, M.A., Rosli, N.A., Gonawan, F.N. & Abdullah, S.J. 2021. Scavenging malachite green dye from aqueous solution using durian peel based activated carbon. *Malaysian Journal of Fundamental and Applied Sciences* 17: 95-103.
- Yusop, M.F.M., Aziz, A. & Ahmad, M.A. 2022a. Conversion of teak wood waste into microwave-irradiated activated carbon for cationic methylene blue dye removal: Optimization and batch studies. *Arabian Journal of Chemistry* 15(9): 104081.
- Yusop, M.F.M., Jaya, E.M.J. & Ahmad, M.A. 2022b. Single-stage microwave assisted coconut shell based activated carbon for removal of Zn(II) ions from aqueous solution - Optimization and batch studies. *Arabian Journal of Chemistry* 15(8): 104011.
- Yusop, M.F.M., Jaya, E.M.J., Din, A.T.M., Bello, O.S. & Ahmad, M.A. 2022c. Single-stage optimized microwave-induced activated carbon from coconut shell for cadmium adsorption. *Chemical Engineering and Technology* 45(11): 1943-1951.
- Zhang, X-X., Xiao, P., Chen, G-J., Sun, C-Y. & Yang, L-Y. 2018. Separation of methane and carbon dioxide gas mixtures using activated carbon modified with 2-methylimidazole. *Chemical Engineering & Technology* 41: 1818-1825.

*Corresponding author; email: chazmier@usm.my